Alignment of Microparts Using Force Controlled Pushing

Wolfgang Zesch, Ronald S. Fearing[1]

Univ. of California, Berkeley, CA 94720, USA
Dept. of Electrical Eng. & Comp. Science (EECS)

ABSTRACT

In today's and tomorrow's development of new products, precise positioning and assembly of small parts is of fundamental importance. Often, such tasks require the alignment of objects with features such as edges or surface structures. In this work, we explore force controlled pushing of microparts on a planar substrate with a micromanipulator. The pushing tool is an AFM cantilever equipped with a piezoresistive force sensor. Its corse position, as well as the global manipulation strategy, is specified by the human operator. First, we present force measurements during typical pushing operations. Using these measurements, a sensor guided controller is implemented to maneuver the robot locally by detecting events such as hitting an obstacle or changing contact conditions. Using force/position macros, we are able to push the objects precisely to a desired location without exceeding a certain limit force. Experimental results demonstrate the ability of aligning microparts on a horizontal plane with micrometer accuracy relative to each other. For automated assembly applications there are two possibilities: the local controller presented in this paper can be integrated either in a passive global positioning system if the geometry of the problem is well defined. Conversely, a feedback system, e.g., with quantitative computer vision, can be used to cover a larger spectrum of object sizes and shapes.

Keywords: pushing, micromanipulation, micropositioning, alignment operation, micropart, force control, force sensing, adhesion, AFM cantilever, microtaction.

---

1. INTRODUCTION

Positioning of workpieces and/or aligning them with other objects is a basic capability needed for automated assembly. Often, it is sufficient to perform this task on a horizontal plane, i.e. with only three kinematic degrees of freedom (DOF). More or less accurate positioning can be the goal itself, or serves as a pre-requisite for the next process, e.g. a 3D assembly operation performed by a robot. The least flexible manipulation strategy is the use of passive fences which re-orient and position parts moving in a vibration feeder or along a conveyor belt [7]. Pick-and-place manipulation, i.e. grasping, transporting and depositing the object with a manipulator arm equipped with a gripper [6][10], allows programmable execution of the positioning task and is well suited for environments clogged with obstacles.

1.1. Pushing

As Mason [12] showed, moving objects by actively pushing them with a manipulator is as flexible, but mechanically less complex than pick-and-place, for planar positioning. It does not require a special grasping tool, nor must the manipulator lift and support the workpieces. Especially important for micromanipulation, the problems of precisely releasing the object is circumvented. Additionally, it is sufficient to access the workpiece from one side or maximally from one half plane, thus facilitating the alignment with walls or other object-sized structures. However, pushing introduces certain restrictions. The moving object is subject to (dry) friction at the contact with the substrate [8]. Previous work has led to a good understanding of pushing with robots, including stability [1][12][14]. In general, these strategies work well for macroscopic parts since the forces involved, such as friction, are well known or can be tightly bounded. Also, the typical accuracy in the millimeter range is relatively easy to achieve. This is not the case in the microscopic domain, i.e., for part dimensions below 1 mm, where adhesion and other surface effects become important.

---

1. Email: (zesch, ronf)@robotics.eecs.berkeley.edu, WWW: http://robotics.eecs.berkeley.edu/(~zesch, ~ronf).

1.2. Micromanipulation

As pointed out by Arai et.al. [2] and Fearing [4], surface tension due to adsorbed water films, electrostatic forces caused by charged particles, and Van der Waals forces become increasingly important at lower dimensions. Often, they exceed the weight of the object. As a result, microparts stick to surfaces, cling together, or even jump to other locations "spontaneously". Various solutions to overcome these problems, mainly during release of the part from the microtool [13][17], but also to actively use these effects [13] have been proposed. As stated by Zesch, the most effective way to reduce the surface forces is to minimize the contact area between tool and workpiece [17]. As a consequence, it is desirable to perform the pushing manipulations with a slim pusher. For macroscopic problems, Coulomb's law is widely used to calculate friction force $\underline{F}_\mu$ and torque $\underline{M}_\mu$ acting on a surface A according to

$$\underline{F}_\mu = \int_A \tau_\mu(\underline{r}) \cdot \frac{\dot{\underline{x}}(\underline{r})}{|\dot{\underline{x}}(\underline{r})|} \cdot dA \quad \text{and} \quad \underline{M}_\mu = \int_A \tau_\mu(\underline{r}) \cdot \frac{\underline{r} \times \dot{\underline{x}}(\underline{r})}{|\dot{\underline{x}}(\underline{r})|} \cdot dA \tag{1}$$

with the friction stress $\tau_\mu(\underline{r}) = \mu(\underline{r}) \cdot p(\underline{r})$. Herein $\mu(\underline{r})$, $p(\underline{r})$, and $\dot{\underline{x}}(\underline{r})$ are the local coefficient of friction and contact pressure, and the relative velocity, respectively at the point $\underline{r}$ of A. Peshkin et.al. presented a method to calculate the center of instantaneous rotation of a pushed object for a given friction distribution $\tau_\mu(\underline{r})$ [14]. While these expressions still hold for microscopic parts, $\mu(\underline{r})$, and even more $p(\underline{r})$ exhibit large local and temporal fluctuations due to roughness, dust particles, humidity or surface charges, as sketched in fig. 1. The force distribution at the contact points as well as their locations are generally unknown. These effects cause a widely moving center of friction (CF), which typically does not coincide with the center of mass (CM). We just know that both CF[2] and CM are enclosed in the convex hull of the polygon spanned by the contact points. Not even the direction of rotation of the pushed object can be calculated safely (compare [12]). In order to stabilize the pushing of microobjects with a point contact it is thus necessary to incorporate sensing and feedback control algorithms.
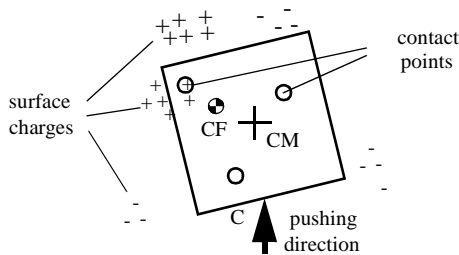

Fig. 1: Pushing an object on an inhomogenous substrate: Surface charges cause large local variation of the friction forces at the contact points and thus an unpredictable location of the center of friction CF.

1.3. Sensor Feedback for Pushing

Planning pushing operations, such as in [12], requires more or less precise knowledge of the initial position, as well as tracking of intermediate locations. This can be achieved by algorithms that inherently reduce position uncertainty [3]. Another way is employing computer vision as a peripheral sensor [5][15]. However, the requirement of visibility places severe restrictions on the manipulation process. Additionally, due to the large computational requirements, it is expensive and slow. These disadvantages are circumvented by tactile sensing [9]. Son et.al. use signals from local force sensors to detect events during manipulation [16] and Lynch et.al. directly incorporate tactile information to control the pushing direction [11].

1.4. Approach

Pushing is a cheap, but nevertheless flexible means of positioning objects. We apply this approach to the microworld. In order to reduce adhesion effects to a minimum (cf. sec.1.2), we will, conversely to macroscopic applications [1], push with a point-contact. Kinematically, this is a decomposition of using a line contact[3]. It guarantees well defined contact conditions and allows the workpiece to move freely in DOFs (lateral slip and rotation) needed for alignment tasks. However, this strategy introduces stability problems, as discussed sec.4. In order to deal with them and to facilitate precise local manipulation, we utilize a tool with an integrated force sensor and explore the environment with active sensing.

The rest of this paper is organized is follows: The first part presents the kinematics of pushing at a point. We show the characteristics of the employed force sensor/tool and evaluate the parameters of pushing in the microscopic domain. Pushing forces are measured and evaluated statistically. The goal herein is to derive algorithms to robustly detect manipulation events from

---

2. but not the real center of friction which lies on a line parallel to F_μ at a distance $|M_\mu|/|F_\mu|$ away from CF, for details cf. [12].

3. A line contact is kinematically equivalent to a two-point contact. In our case, both points fall together.

the force signal. In the second half of the paper, we apply this knowledge to implement basic local manipulation macros. As a benchmark test, we demonstrate the system's ability to push silicon blocks stably in a straight line and align them with other structures on the substrate. Finally, we conclude with a discussion of the potentials and limitations of the presented pushing strategies and propose possible solutions.

2. THE PUSHING SYSTEM

As discussed above, in this work we investigate pushing of microparts with a single point. Throughout the paper, we use the notation of [11] (cf. fig. 2a). A workpiece W is pushed by the pusher P at a point C along the y-direction of a fixed coordinate
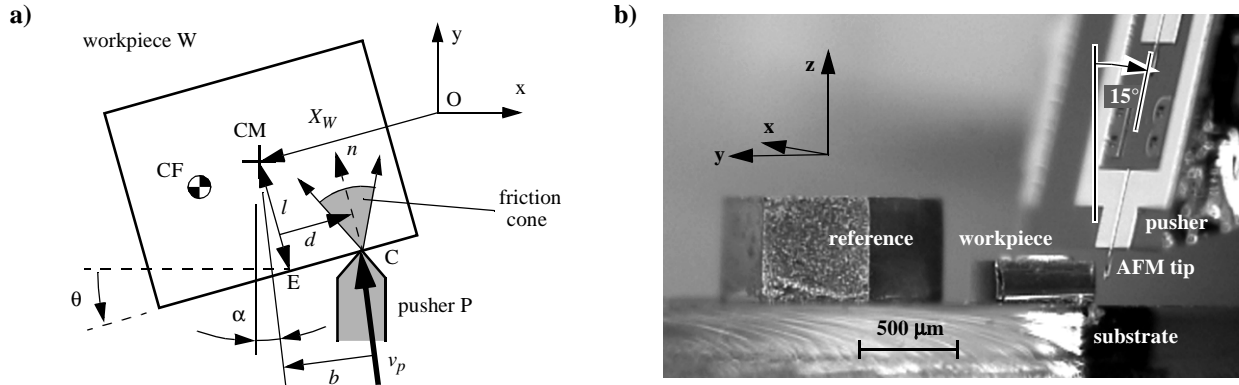
Fig. 2: Pushing system, a) *geometry (top view),* **b)** *side view showing the pusher (AFM cantilever), a workpiece (500 × 500 × 200 mm³ silicon block), and a reference object resting on the substrate (silicon wafer).*

system O with a velocity v_P, which includes an angle α with the y-axis. P touches W at a distance d from E, the contact edge's closest point to the center of mass CM of W[4]. The CM typically does not coincide with the (unknown) location of CF, but is used as an approximation to estimate the torque

$$M_P \approx F_P \cdot b = F_P \cdot l \cdot \sin(\theta - \alpha) + d \cdot \cos(\theta - \alpha) \tag{2}$$

applied to the part by off-center pushing with a lever arm b. θ denotes the angle of the pushed edge against the y-axis and n its normal unit vector. The coefficients of friction between W and P on one side is μ_c, and between W and substrate is μ_s. The

force-sensitive pusher was implemented with a piezoresistive AFM cantilever[5] (fig. 2b). Its dimensions are 150 µm × 50 µm × 3 µm (length × width × thickness). The stiffness along its sensitive direction amounts to 8 N/m. Together with a standard strain-gauge amplifier it shows a sensitivity of 0.27 V/µN with a RMS noise level of less than 0.1 µN and a bandwidth of 2 kHz. The cantilever is tilted 15° about the x-axis in order to guarantee a well defined point contact. A beneficial side effect of this inclination is the – though much smaller – sensitivity in z-direction which is used for approaching the substrate plane and for safety routines. As workpieces we chose silicon diodes, basically blocks of 500 µm × 500 µm × 200 µm, with a weight of 1.1 µN (fig. 2, b). Their contact surface with the substrate is the rough unpolished back side of a silicon wafer with a roughness R_a < 3 µm.
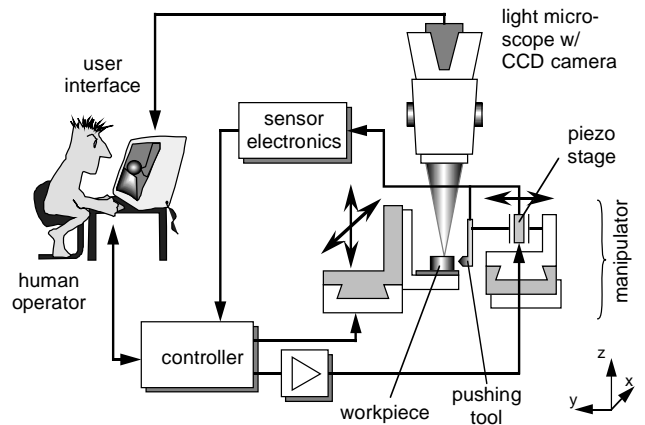

Fig. 3: Sketch of the manipulator used for the experiments.

---

4. In our case, for the silicon 500 micron square blocks, E is the center of the front (pushed) edge of W.
5. Piezolever from Park Scientific Instruments, Palo Alto, CA, www.park.com.

The pusher-workpiece contact point C is fixed at about 120 μm above the substrate. With sufficient accuracy, we can thus treat the system as a two-dimensional problem in the pushing plane. W's position can be expressed by its coordinates $X_W = [x_w, y_w, \theta]$. An equivalent notation is given by the location X_E of E and the edge angle θ. As the substrate, we used a piece of a silicon wafer. Its optically flat surface (native oxide) was cleaned firstly with acetone and subsequently with alcohol before each measurement sequence. The substrate is moved in x- and z-direction by a micrometer stage driven by stepper motors with a resolution and a backlash of 0.6 μm and 7 μm, respectively. The robot works under a stereo microscope and is tele-operated by a human operator via a dedicated user interface, as sketched in fig. 3.

Pushing forces were monitored with the force sensor system, positions were gained from a capacitive proximity sensor for the y-direction (± 1 μm / 15 kHz) and by counting the signals sent to the stepper motors. W's position and orientation X_W relative to the tool were extracted from the position/force signals using a repeated-probing algorithm. Alternatively, orientations were manually inferred from the top view video image ($\pm 2°$). Monitoring of both temperature T and relative humidity HR during experiments showed a range of 22…27°C and 45-58%, respectively.

3. FORCES DURING PUSHING

In order to characterize the system's behavior we performed several test motions. The force acting between tool and part during typical pushing operations with $v_P = 0.2$ m/s for two different contact locations ($d = 0$ and 0.2 mm) with a starting angle $\theta_0 = 0$ is shown in fig. 4, a). After the approach phase, the pushing force F_P jumps to a peak values of up to 8 μN. After the break-away/acceleration phase, F_P quickly drops to typically 0.8…3.5 μN. In this phase, one can clearly observe stick-slip manifested by a slow building-up followed by a rapid drop of F_P. This effect can even cause separation of tool and micropart.
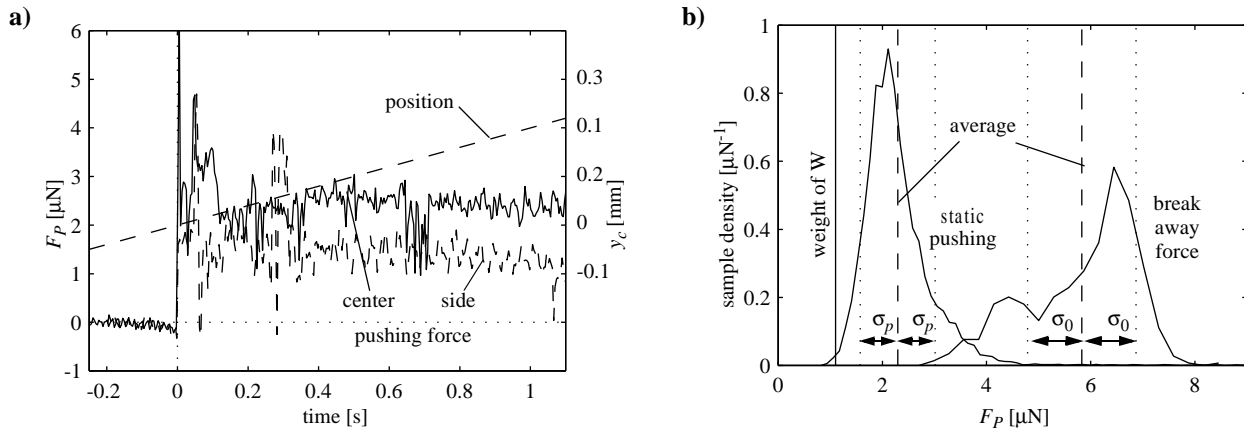

Fig. 4: Force during pushing a 1.1 μN block at $v_P = 0.2$ mm/s. a) pushing at the center and at the side of the pushed edge, b) distribution of the pushing force of 10 different 0.1 mm-pushes with 1000 samples each. The continuous and the dotted lines indicate the average and the standard deviation of the force distribution, respectively.

The average force needed to move the parts along the substrate as well as the break-away force vary as much as a factor of 5 from one day to the other. We blame the changing environmental conditions for these large fluctuations (cf. sec.1.2). However, single measurement sequences generally showed a standard deviation of less than 25% of the average value. We will discuss the extraction of pushing events from this noisy signal later. Another important factor for the size of F_P is the location d of the contact C. As shown in fig. 4, a) the force drops to about 50% for $d = 0.2$ mm (40% of the part width) compared to pushing at the center. A typical sample of 10^4 measurements of F_P for constant velocity ($\dot{y}_P = 0.2$ mm/s) and the break-away force F_{P0} show mean values at 2.2 μN and 5.8 μN, respectively (cf. fig. 4b) and standard deviations σ_p and σ_0 of 25% of the mean.

With the assumption of power dissipation by friction, i.e.,

$$\dot{\theta} \cdot M_\mu = -\dot{\theta} \cdot M_P \leq 0 \quad \Leftrightarrow \quad \dot{\theta} = k \cdot M_P, \quad k \leq 0 \tag{3}$$

eq. (2) indicates that the system is unstable for $l > 0$ and small θ.

Small deviations from the equilibrium angle $(\Rightarrow b = 0)$, i.e., inhomogenities in the distribution of the friction force, mis-alignements and imperfect tool motion quickly lead to large errors in orientation. Fig. 5a demonstrates the θ-trajectory of 5 central pushing operations starting at $\theta_0 \approx 0°$. The distribution of final orientations of a sample of 50 pushes with a pushing length $\Delta y_P = 500 \ \mu m$ is shown in fig. 5b.
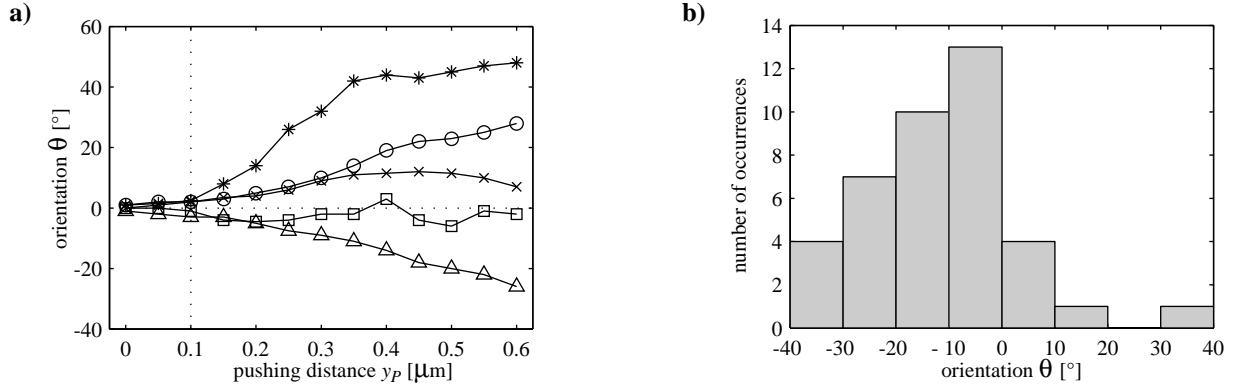
a)

b)

Fig. 5: Orientation of the part after pushing, **a)** *evolution of the angle* θ *during different approaches,* **b)** *distribution of* θ *after a 0.5 mm long push with* $\theta_0 \approx 0°$.

Our manipulation algorithms detect the mis-orientation by probing and select the contact location d accordingly, as discussed in the next section. We define a maximum orientation error during a pushing task of $\theta_{max} = \pm 6°$ which results in a maximum push step size of $\Delta y_{P, max} = 100 \ \mu m$.

4. BASIC PUSHING MACROS

In this section, we present a finite state machine (FSM) which controls the position/orientation X_W of the object W to the goal $X_{W, des}$ by tracking the contact point C. Therefore, the controller estimates y_c, x_c, and θ in-process relying on the detection of contact events and signals from the robot's joint sensors. At the begin of each pushing sequence, a special find-macro provides information about the initial configuration.

4.1. Orienting the part

Before an object can be pushed along a desired direction using a point-contact tool it must be oriented as close as possible to its equilibrium position, i.e., $b \approx 0$. This operation is not only necessary at the begin of a pushing sequence, but becomes even more important during its execution to correct for the accumulated errors. Generally, rotating the part is performed optimally with as large a lever arm b as possible.
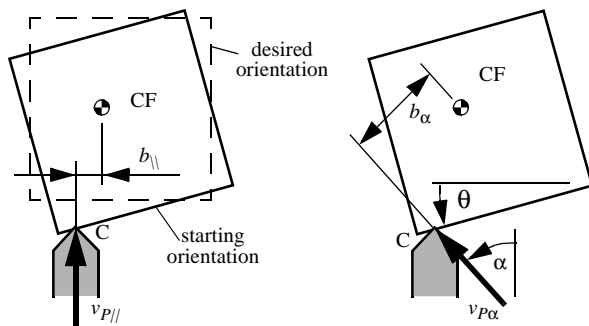

Fig. 6: Orienting by pushing parallel to the main direction (left) and with an angle α *(right).*

Tab. 1: Orienting parts with different pushing directions α, *starting angle* $\theta_0 = 30°$, *pushing distance* $\Delta y_P = 0.2 \cdot \sin 30° = 0{,}1 \ mm$.

pushing angle α	final orientation θ_f	pushing offset Δx_c / Δy_c
[°]	[°]	[μm]
0	19.8±3.93	50 / 48
30	15.4±2.33	67 / 33
45	9.8±5.06	105 / 7

Fig. 6 illustrates this relation for parallel pushing as well as for an angle α. Care has to be taken at the selection of α: The force applied by the tool P at C must lie inside the friction cone ($\mu_c = 0.5 \ldots 2.5$) to avoid slip between W and P, i.e., the relation

$$-\mu_c \le \tan(\alpha - \theta) \le \mu_c \tag{4}$$

has to be satisfied. For a more detailed discussion cf. [12].

The results of turns with $\alpha = 0°$, $30°$, and $45°$ are summarized in table 1. W was pushed $|d| = 0.2$ mm left and right of the center from a starting "mis"-orientation of $\theta_0 = \pm30°$. The pushing distance Δy_P was set to the theoretical value for straight-ening ($0.2 \times \sin 30° = 0.1$ mm) and a lateral component of $\Delta x_P = \Delta y_P \cdot \tan\alpha$ was added to the P's motion. In agreement with the theoretical considerations, the turning is significantly more efficient with larger angles α. At the same time, the offset in y-direction Δy_c decreases, indicating a reduced y-distance of the center of rotation from the center of mass CM. However, too large an angle raised the likelihood of P slipping along the pushed edge. Repeatedly, W was missed, requiring an extra x-adjustment step. As a result, we selected a pushing angle α for re-orientation of $30°$.

4.2. Straight pushing

Initial mis-orientations of $\pm30°$, as well as the large uncertainties in friction render it impossible to directly move parts W to a desired position in one single step or in a predictable way (cf. fig. 5). Hence, we utilize the aforementioned method to re-orient the W after each pushing step. Depending on θ, the FSM controller decides whether to push either at the center or at the left or right end of the pushed edge. The value of θ also determines the pushing angle α.

Fig. 7a shows the results of $250 \ldots 350$ µm long pushing operation to the goal at $[x_c, y_c, \theta]_{des} = [0.5$ mm, 0 mm, $0°]$. According to fig. 5, the steps Δy_P were limited to 100 µm, although they can actually be much smaller, depending on the orientation error. As the reader can see in fig. 7b, repeated off-center pushes (dashed lines) generally bring the orientation towards 0 while central pushes (continuous lines) tend to destabilize the system. However, central pushing facilitates larger steps. Provided θ is small ($\pm6°$), they are thus used for fast motions. The straight-pushing algorithm consists of both stabilizing re-orientations and sub-critical central pushes. As a result, we are able to maneuver the 500 micron-sized workpieces with initial orientations of $|\theta_0| < 30°$ to the goal achieving a final accuracy of 7 µm / 2°.

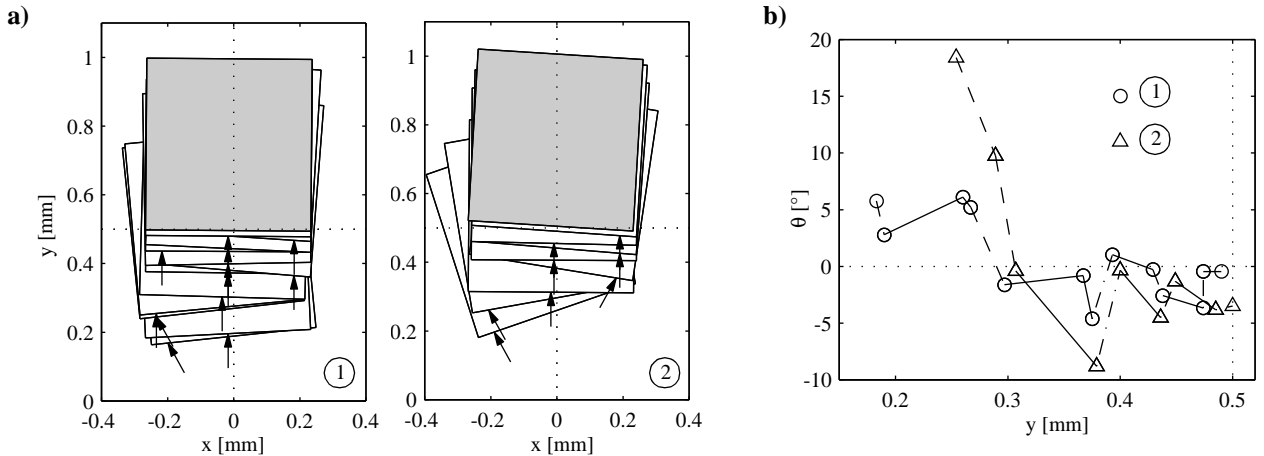*Fig. 7: Straight pushing of the silicon block.* **a)** *Sequence of sub-motions to the goal ($y_c = 0.5$ mm, $\theta = 0°$). The squares indicate intermediate positions and the arrow the pushing point C and the pushing direction, respectively,* **b)** θ *-trajectories of the sequences shown on the left side. Continuous lines mark pushing at the center of W, dashed lines indicate contact at the side of the pushed edge.*

Due to non-holonomic constraints inherent to pushing with a point-contact, X_W is locally uncontrollable. Thrusting at different edges of W is not applicable since our tool is not sensitive in this direction and thus would not provide any reliable contact information. A strategy would be the integration of additional DOFs to turn either the tool or the substrate carrier, thus allowing the robot to apply forces along arbitrary (in-plane) directions. The discussion in this paper is restricted to pushing at one edge. However, the results are applicable for general pushing directions as well.

4.3. Alignment with an object/wall

If one part has to be aligned precisely with a target part without moving the target from its reference position or with a delicate feature such as a low-thickness surface structure[6], local force information has to be used. Here, we assume that the part W is already roughly positioned in front of the reference structure R. This could have been done either by a larger robotic manipulator or with previous pushing operations (cf. sec.4.1 and sec.4.2). The presented algorithm then positions W such that it touches R and that its orientation matches the front edge of R. As in sec.4.2, accurate lateral positioning can be achieved by a robot equipped with additional DOFs.

Fig. 8a shows the result of a straight, sensorless pushing operation. Firstly, P pushes just W until W touches and subsequently displaces R. In our experiments R was a silicon hexagon with the side length of 530 μm and a height of 380 μm. From the force trajectory, we can clearly identify the contact events, the acceleration phase, and finally the displacement of R.
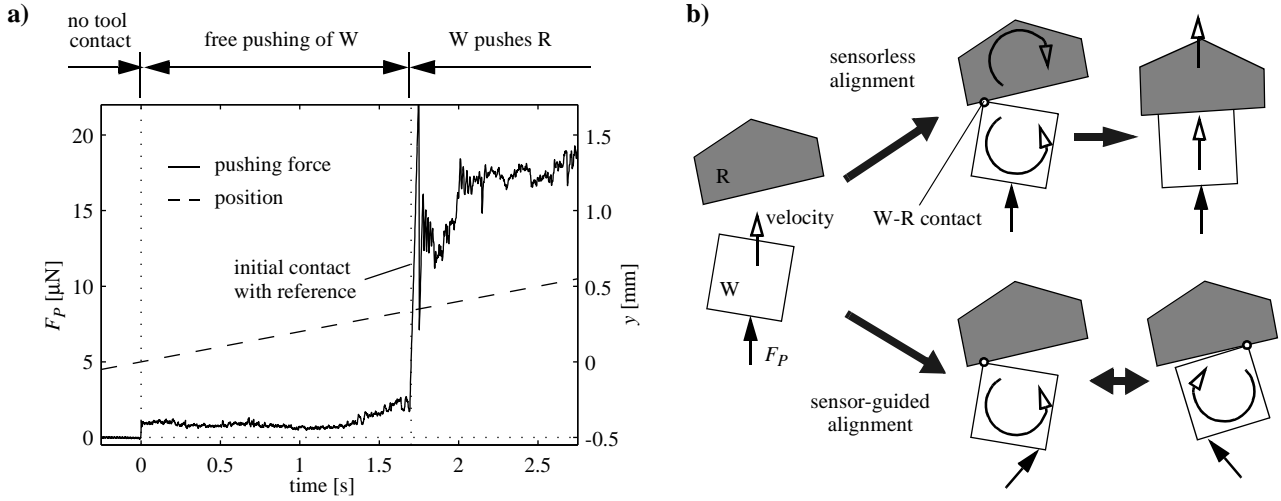

Fig. 8: Alignment of two microobjects by pushing. **a)** *Pushing force during uncontrolled alignment of a microobject W with a moveable reference part R. At contact time (1.7 s), the average force increases from 1.5 μN to about 16 μN.* **b)** *Comparison of sensorless and sensor-guided alignment: While in sensorless alignment (upper path) a rotation of R can merely be avoided, in the sensor-guided version (lower path) the force information is used to detect contact events and subsequently switch to the appropriate pushing configuration.*

This behavior is sketched in the upper half of fig. 8b. In order to avoid any displacement (or damage) of R, the controller has to (1) immediately identify the touching event and to (2) choose an appropriate pushing angle α. The first task is solved by adaptive thresholding, i.e., we track the average of the pushing force F_P with a slow low-pass filter ($\tau_{slow} = 50$ ms) and compare this signal to the force input filtered with a faster filter for noise reduction ($\tau_{fast} = 2$ ms). The contact transition event is fired when the ratio of these two signals exceeds a predefined value. To finally align W with R, the algorithm follows an iterative strategy consisting of alternative left and right orientations (cf. sec.4.1), thereby benefiting from their intrinsic offset in *y*-direction. In doing so, it minimizes the force between W and R and thus avoids undesirable displacements of R.

For our experiments, we performed several alignment processes with the same, unchanged reference position starting from different, manually arranged initial positions with $|\theta_0| < 10°$. At the end of each alignment sequence we calculated the reference position using W's (theoretical) geometry and final position. The mean of all calculated positions of R served as the ground truth to evaluate the accuracy of the alignment process. An example of such a sequence is shown in fig. 9a. Fig. 9b depicts the top view of the corresponding initial (left) and final (right) configurations. To summarize, a series of 5 alignment processes resulted in an uncertainty of 2.89 μm and 0.090° in y- and θ-directions, respectively.

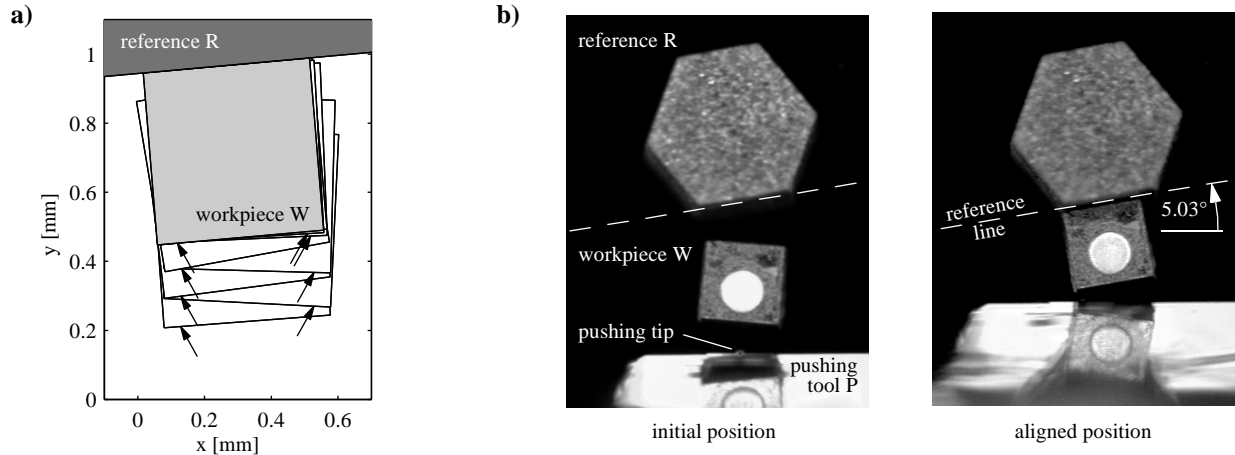6. e.g. microfabricated mechanical structures or a thin layer of aluminum or photo resist

Fig. 9: Push-alignment of a micropart W with a (moveable) reference object R, **a)** *pushing sequence,* **b)** *top view of the initial (left) and final (right) arrangement. As the ground truth for the reference position we calculated the average position from 5 independent alignment sequences.*

5. DISCUSSION

A large problem is the instability of pushing with a single point contact. While this manipulation strategy greatly reduces the sticking of W to P, it also makes it more difficult for the controller to follow a desired trajectory. A solution would be the employment of a double point tool. This new configuration still retains a small contact area and thus a low sticking tendency. On the other hand, it possesses characteristics similar to pushing with a (linear) fence of the same width, which stabilizes the system passively. Furthermore, two sensors, one in each tip, provide contact torque information and thus allow the controller to anticipate erroneous object rotations.

In about 30% of the pushing sequences we noticed sudden, unpredictable motions of W caused by rapid and vast changes of the location of CF. Most of these disturbances could be corrected by our FSM controller (cf. sec.4). However, due to the non-holonomic nature of the task, the manipulator was not able to compensate large position errors close to the goal. To resolve this problem, the robot has to be equipped with additional DOFs (cf. sec.4.2). A different recovery strategy would be repositioning W with another robot and performing a next trial. Therefore, failure has to be detected reliably, e.g., with the built-in force sensors. To circumvent the aforementioned problem at its root, ways to limit the change in contact parameters have to be found. Due to the rather high roughness of our parts (< 3 μm), mainly electrostatic and capillary force are to blame for the unpredictable behavior (cf. fig. 1). Work under controlled conditions (temperature and humidity) or in a liquid bath, as well as coating the surfaces with conductive layers are often proposed to reduce these effects [2][4]. High-frequency vibration of the substrate would reduce the contact time and thus reduce the net friction as well.

Finally, if the local pushing works sufficiently reliable, it has to integrated into larger system. Rough positions of R and W can be provided by a human operator in tele-operation (as performed in this work) or by a peripheral sensor, such as vision [5][15].

6. CONCLUSION

Compared to other manipulation strategies, active pushing of objects possesses several advantages such as flexibility, simplicity of the robot tool, easy accessibility of the workpiece, and the absence of actuators to lift it. In this work we applied the principle of pushing to the microworld. In order to minimize adhesion between tool and object, but also to allow the objects to passively align with features subject to uncertainty, the pushing was performed with a point contact. An integrated force sensor provides information about the contact force. The typical range for pushing silicon blocks with a weight of 1.1 μN with a constant speed of 0.1…0.3 mm/s along a silicon wafer was 0.8…3.5 μN with a break-away force about twice as high. Significant changes in the pushing force from one day to the other made it necessary to track the mean force and to use adaptive thresholding for event detection. Using this technique, the controller was able to react reliably on events such as touching, loss of object

and hitting fixed or heavy obstacles. Relying on this event detection, we programmed simple macros to maneuver microparts locally. Together with a re-orienting procedure, the controller was able to stably move the parts to a desired position with 7 µm / 2° accuracy. The alignment macro is able to align workpieces with a moveable or fragile reference structure with an uncertainty of less than 3 µm / 0.1°. The success ratio of our algorithms was about 90%, but can be improved significantly by changing the robots kinematic design.

7. ACKNOWLEDGEMENTS

8. REFERENCES

1. Akella S., Mason M.T.," Parts orienting by push-aligning", *IEEE Int'l Conf. on Rob. & Autom. ICRA '95*, vol.1:414-420, May 1995, Nagoya, Japan.
2. Arai F., Andou D., Fukuda T., Nonoda Y., Oota T., "Micro manipulation based on micro physics-strategy based on attractive force reduction and stress measurement", *IEEE/RSJ Conf. on Intell. Robots and Systems IROS '95*, vol 2:236-241, 1995, Pittsburgh, USA.
3. Erdmann M.A., Mason M.T., "An exploration of sensorless manipulation", *IEEE J. of Rob. & Autom.*, vol.4(4):369-379, Aug. 1988.
4. Fearing R.S., "Survey of sticking effects for micro parts handling", *IEEE/RSJ Conf. on Intell. Robots and Systems*, vol.2:212-217, Pittsburgh, PA, 1995.
5. Feddema J.T., Keller C.G., Howe R.T.," Experiments in micromanipulation and CAD-driven microassembly", *SPIE Conf. on Microrobotics and Microsystem Fabrication*, vol.3202:98-107, Oct. 1997, Pittsburgh, PA, USA.
6. Greitmann G., Buser R.A., "Tactile microgripper for automated handling of microparts", *Transducers 95 - Eurosensors IX, 8th Int'l Conf. on Solid-State Sensors & Actuators*, vol.2:372-375, June 1995, Stockholm, Sweden.
7. Goldberg K., Peshkin M., Brokowsky M., "A complete algorithm for designing passive fences to orient parts", *Assembly Automation*, vol.17(2):129-136, MCB Univ. Press, 1997.
8. Goyal S., Ruina A., Papadopoulos J., "Planar sliding with dry friction. Part 1: Limit surface and momentum function", *Wear*, vol.143(2):307-330, 1991.
9. Howe R.D., "Tactile sensing and control of robotic manipulation", *Advanced Robotics*, vol.8(3):245-261, 1994.
10. Keller C.G., Howe R.T.," Hexsil tweezers for teleoperated micro-assembly", *IEEE 10th Int'l Workshop on MEMS, An Investigation of Microstructures, Sensors and Actuators, Machines and Robots*, p.72-77, Jan. 1997, Nagoya, Japan.
11. Lynch K.M., Maekawa H., Tanie K., "Manipulation and active sensing by pushing using tactile feedback", *IEEE/RSJ Int'l Conf. on Intell. Robots and Systems IROS '92*, p416-421, July 1992, Raleigh, NC, USA.
12. Mason M.T., "Mechanics and planning of manipulator pushing operations", *Int'l J. of Rob. Res.*, vol.5(3):53-71, 1986.
13. Miyazaki H., Sato T., "Fabrication of 3D quantum optical devices by pick-and-place forming", *IEEE 9th Int'l Workshop on MEMS*, p318-324, Feb. 1996, New York, NY, USA.
14. Peshkin M.A., Sanderson A.C., "The motion of a pushed, sliding workpiece", *IEEE J. on Rob. & Autom.*, vol.4(6):569-598, 1988.
15. Pappas I., Codourey A., "Visual control of a microrobot operating under a microscope", *IEEE/RSJ Int'l Conf. on Intell. Robots and Systems IROS '96*, vol.2:993-1000, Nov. 1996, Osaka, Japan.
16. Son J.S., Monteverde E.A., Howe R.D., "A tactile sensor for localizing events in manipulation", *IEEE Int'l Conf. on Rob. & Autom. ICRA '94*, vol.1:471-476, May 1994, San Diego, CA, USA.
17. Zesch W., Brunner M., Weber A., "Vacuum tool for handling microobjects with a nanorobot", *IEEE Int'l. Conf. on Rob. & Autom. ICRA '97*, vol.2:1761-1766, April 1997, Albuquerque, NM, USA.
18. Zhou Y., Nelson B., Vikramaditya B., "Fusing force and vision feedback for micromanipulation", *IEEE Int'l Conf. on Rob. & Autom. ICRA '98*, vol.2:1220-1225, May 1998, Leuven, Belgium.